PCCP

Field-enhanced bulk conductivity and resistive-switching in Ca-doped $BiFeO_3$ ceramics

Journal:	*Physical Chemistry Chemical Physics*
Manuscript ID:	CP-ART-06-2014-002580.R1
Article Type:	Paper
Date Submitted by the Author:	01-Aug-2014

Complete List of Authors:	Maso, Nahum; University of Sheffield, Department of Engineering Materials Beltran, Hector; Jaume I University, Prades, Marta; Universitat Jaume I, Departamento de Química Inorgánica y Orgánica Cordoncillo, Eloisa; Jaume I University, Inorganic Chemistry West, A; University of Sheffield, Department of Engineering Materials

Field-enhanced bulk conductivity and resistive-switching in Ca-doped $BiFeO_3$ ceramics

Nahum Masó[1], Hector Beltrán[2], Marta Prades[2], Eloisa Cordoncillo[2] and Anthony R. West[1]

[1] Department of Materials Science and Engineering, University of Sheffield, Mappin Street, S1 3JD Sheffield, United Kingdom.

[2] Departamento de Química Inorgánica y Orgánica, Universitat Jaume I, Avda. Sos Baynat s/n, 12071 Castellón, Spain.

Abstract

The bulk conductivity at room temperature of Ca-doped $BiFeO_3$ ceramics is *p*-type and increases reversibly by up to 3 orders of magnitude under the influence of a small *dc* bias voltage in the range ~3 to 20 Vmm^{-1}. The effect occurs in both grain and grain boundary regions, is isotropic and does not involve creation of filamentary conduction pathways. It is proposed that, by means of capacitive charging and internal ionisation processes under the action of a *dc* bias, hole creation leads to a more conductive excited state. This gradually returns to the ground state when the *dc* bias is removed and the holes recombine with electrons trapped at the sample surface. The holes are believed to be created on oxygen, as O^- ions.

Introduction

The memory-sensitive resistor, or memristor, [**1–3**] has attracted substantial interest because of its potential memory applications in electronic circuits. This was postulated in 1971 as the fourth basic circuit element [**1**] – alongside the resistor, capacitor, and inductor – and is characterized by a voltage-dependent resistance with memory. Devices showing electrically-induced resistive switching usually consist of metal│insulator│metal thin film sandwiches [**4–10**], where the insulator material ranges from binary or more complex oxides and chalcogenides to organic compounds.

Bismuth ferrite ($BiFeO_3$) has also attracted considerable attention in recent years since it exhibits both G-type antiferromagnetic order with a long-periodicity spiral below the Néel temperature (~367 ^oC) and ferroelectricity below the Curie temperature (~827 ^oC); these two effects together may allow fabrication of novel functional materials that involve coupling between magnetic and electrical order.

Recently, Rubi *et al.* [**11,12**] reported resistive-switching in $Bi_{0.9}Ca_{0.1}FeO_3$ ceramics that was associated with a Schottky barrier at the sample–electrode interface, i.e. it behaves as a metal–oxide varistor. We report here a very different effect: resistive-switching in Ca-doped $BiFeO_3$ ceramics is observed in both grain and grain boundary regions and is several orders of magnitude greater than that reported to be associated with the Schottky barriers. In particular, the bulk conductivity at room temperature is enhanced, reversibly, by up to 3 orders of magnitude under the influence of a small *dc* bias voltage. A new switching mechanism for this phenomenon is proposed.

Experimental

Samples of two compositions, $Bi_{0.95}Ca_{0.05}FeO_{2.975}$ (BCF05) and $Bi_{0.70}Ca_{0.30}FeO_{2.85}$ (BCF30), were prepared by solid state reaction using powders, and drying temperatures, of Bi_2O_3 (99.99% pure, Acros Chemicals, 180 °C), $CaCO_3$ (99% pure, Sigma-Aldrich, 180 °C) and Fe_2O_3 (99% pure, Sigma-Aldrich, 400 °C). These were mixed in an agate mortar and pestle for ~30 min, with acetone added periodically to form a paste. Pellets were pressed and placed on sacrificial powder of the same composition in alumina boats. Initial firing was at 850 °C for 20 min to eliminate CO_2 after which the pellets were ground, repressed, fired again at 850 °C for 20 min and reground. Pellets (~0.5 g, ~1.5 mm thick, ~6.5 mm diameter) and bars (~0.7794 g, ~3.95 mm width, ~4.0 mm height, ~7.90 mm length) were then prepared, pressed isostatically at 200 MPa, fired at ~850–945 °C for 2 h in air and cooled slowly by switching off the furnace.

The phases present were analysed by X-Ray Powder Diffraction (XRD) using a Stoe StadiP Diffractometer, $CuK\alpha_1$ radiation with a linear position-sensitive detector; lattice parameters were determined by least-squares refinement for reflections in the range $15 < 2\theta < 80^o$, using the software WinXPow version 1.06, and an external Si standard.

For electrical property measurements, samples (pellets and bars ~95 % dense) were coated with electrodes made from Pt paste that was decomposed and hardened by heating to 800 ºC for 1 h; for selected experiments, Ag paint and an In/Ga alloy were used also as electrodes. On pellets impedance measurements used a combination of Agilent 4294A and E4980A impedance analysers over the frequency range 40 Hz to 2 MHz, with an *ac* measuring voltage of 0.1 V and over the temperature range –263 to 65 ^oC; for subambient measurements, an Oxford Cryostat with Intelligent Temperature Controller (ITC 503S) was used. For selected experiments, impedance measurements were made at the same time as a small *dc* bias voltage was applied across the sample. On bars, dc bias voltages (Stanford Research Systems, model PS350/5000V-25W) were applied and the current (Stanford Research Systems, model PS350/5000V-25W) and the conductivity (Keithley 2000) were

measured both parallel and perpendicular to the direction of the dc bias, respectively. Impedance data were corrected for blank permittivity of the conductivity jig and for overall pellet geometry. Therefore, resistivity and permittivity data are reported in units of Scm^{-1} and Fcm^{-1}, respectively. Resistivity values were obtained from intercepts on the real, Z' axis.

Results

Samples of $Bi_{1-x}Ca_xFeO_{3-x/2}$: x = 0.05 (BCF05) and x = 0.30 (BCF30) were single phase by XRD after firing at 925 and 945 °C, respectively. The pattern of BCF05 was indexed and refined on a rhombohedral unit cell with a = 5.578(1), c = 13.850(3) Å, whereas that of BCF30 was indexed and refined on a cubic unit cell with a = 3.9203(2) Å.

In order to characterise the electrical microstructure of the samples, variable frequency impedance measurements were made on pellets heated in air and cooled slowly to room temperature by switching off the furnace. Although a full characterisation of the electrical properties of BCF ceramics has been published [**13**], we indicate here the main characteristics to demonstrate that true sample impedances were measured rather than interfacial Schottky barriers. Impedance data for BCF05 contained two arcs from which resistivity values R_1 and R_2 were obtained from intercepts on the real Z' axis, **Figure 1(a,b)**. From the magnitudes of the associated permittivity values, C_1 represented the bulk permittivity of the sample, e.g. ~6 $pFcm^{-1}$ at –73 ^oC, whereas C_2 was of the order of nanofarads and was attributed to a conventional grain boundary. By contrast, BCF30 showed a single, almost ideal, arc, **Figure 1(c,d)**, indicating that the sample was electrically homogeneous and could be represented, ideally, by a single parallel RC element in which R represents the bulk resistivity and C represents its permittivity. The bulk permittivity of BCF30 increased from ~6 to ~12 $pFcm^{-1}$ with increasing temperature from –263 to 27 ^oC; these permittivity values are comparable to those reported previously [**14,15**]. Since, for both compositions, there was no evidence of any additional impedance associated with charge transfer processes at the sample−electrode interface and the conductivity increased with oxygen partial pressure during measurement, the principal conducting species were electronic and, in particular, the conduction mechanism was *p*-type [**13**]. Bulk resistivity (R_1) data give linear Arrhenius conductivity plots in **Figure 2** with activation energies of 0.36(2) and 0.45(1) eV.

In order to study the effects of an applied *dc* bias voltage on the *ac* electrical properties, impedance measurements were made, at room temperature, ~25 °C at the same time as a small *dc* bias voltage, in the range 5 to 30 V, was applied across the pellet. For a typical pellet thickness of ~1.5 mm, these voltages corresponded to a voltage gradient of ~33 to 200 Vcm^{-1}. The impedance data,

presented as both impedance complex plane plots, **Figure 3 (a,b)** and as log admittance, Y' against log frequency **(c,d)**, were very different without, and with *dc* bias. With a *dc* bias, the resistivity of the sample decreased before reaching a steady state, whose total resistivity, in the range ~50–100 Ωcm, was about 3 orders of magnitude less than the initial resistivity ~ 10^5 Ωcm. With increasing temperature, in the range 20–60 °C, a similar decrease in resistivity on application of a *dc* bias was observed.

In **Figure 4**, Arrhenius plots of total conductivity for BCF05 measured without a *dc* bias and after reaching a steady state with an applied voltage of 192 Vcm^{-1} are dramatically different. Without a *dc* bias, plots are linear with activation energy ~ 0.44(1) eV, whereas with a *dc* bias, data exhibit curvature at high temperatures but with almost zero activation energy at low temperatures.

Conductivity data are shown against time at the same temperature, 27 °C, for two different applied voltages in **Figure 5** (for BCF05) and at two temperatures for two different voltages in **Figure 6** (BCF30). For both sets of data, conductivity increased rapidly at first before levelling off at an approximate plateau after short times, but then increased again, this time increasingly rapidly, and finally levelled off. At e.g. 27 ^oC, both the grain and grain boundary conductivity of BCF05 increased over a period of ~55 minutes and then levelled off with 118 Vcm^{-1} bias, whereas a steady state was reached after a few minutes with 137 Vcm^{-1} bias, **Figure 5**. Thus, the time taken to achieve a steady state depended on the magnitude of the applied bias. On increasing temperature, the magnitude of the applied voltage required to achieve a steady state within a few minutes decreased, as shown for BCF30 in **Figure 6**. In all cases, the increase in conductivity on application of a *dc* bias was reversed on removal of the *dc* bias and the samples regained their original state, **Figures 5** and **6**; but, the time taken to recover the original state was almost composition- and temperature-independent. The voltage-dependent resistivity is, therefore, associated with both grain boundary (BCF05) and, importantly, bulk (BCF05 and BCF30) electrical components. It is also independent of electrode material: results obtained with Ag and In/Ga electrodes (not shown) were similar to those reported here with Pt electrodes.

In order to determine whether the conductivity increases were confined to the direction of the applied bias, experiments were conducted on a bar of BCF30, **Figure 7(a)** inset. After a *dc* bias was applied, the current and the conductivity were measured both parallel and perpendicular to the direction of the *dc* bias, respectively. Both conductivity and current increased with time until the current was limited by the instrumentation to 5.5 mA, **Figure 7(a,b)**; subsequently, on removal of the bias, the conductivity recovered its original state, **Figure 7(b)** inset. Both the conductivity

increase and the recovery time observed in bar samples were comparable to those observed in pellets, **Figures 5** and **6** showing that the mechanism associated with the conductivity increase is exhibited by the sample as a whole, rather than filamentary and is isotropic rather than uni-directional. All subsequent data reported here were obtained on pelleted samples.

Data for the total conductivity at three temperatures for the two compositions as a function of applied voltage are shown in **Figure 8**. For each measurement, the voltage was maintained constant until a steady state was reached. On increasing the applied voltage, the steady state conductivity increased slightly at first, but then at the **onset voltage**, increased suddenly by about three orders of magnitude and achieved an approximately constant value. On subsequently decreasing the applied voltage, the high conductivity state was retained, with significant hysteresis, until an abrupt transition to the original state occurred. The voltage at which this transition occurred is referred to as the **twilight voltage**. The onset voltage decreased with increasing temperature whereas the twilight voltage was independent of temperature in the range ~20–50 °C, with a value ~40 Vcm^{-1}. The conductivity (σ) *vs* voltage (V), hysteresis loop became narrower at the waist, therefore, on increasing temperature.

Total conductivity data against temperature for a range of applied voltages are shown in **Figure 9**; the shape of the conductivity-temperature profile is voltage-dependent. The anomalous increase in conductivity at the onset voltage was not seen with zero dc bias (a) but occurred increasingly sharply, and at lower temperature, with increasing bias. Thus the onset voltage was tunable depending on temperature. On cooling, the sample either regained its original state (b) or remained excited (c) until the *dc* bias was removed, depending on whether the applied voltage was greater or smaller than the twilight voltage referred to above.

Finally, conductivity data measured in air, N_2 and O_2, against time, after a voltage of 70 Vcm^{-1} was applied, are shown in **Figure 10**. No significant dependence of the conductivity-time profile on atmosphere during measurement was observed, indicating that oxygen exchange between sample and the atmosphere is not primarily responsible for the conductivity changes with/without *dc* bias.

Discussion

A homogeneous solid solution forms with Ca^{2+} ions dissolved in the $BiFeO_3$ lattice and charge compensation by creation of oxygen vacancies. The $Bi_{1-x}Ca_xFeO_{3-x/2}$ ceramics studied here are *p*-type semiconductors with bulk conductivity $\sim 1\times10^{-3} - 4\times10^{-5}$ Scm^{-1} at room temperature and activation energy ~0.40(5) eV. The *p*-type conductivity has previously been attributed to the

presence of Fe^{4+}ions, although this has not been proved [**13**]. However, the *p*-type conductivity is enhanced by up to 3 orders of magnitude at room temperature and by many orders of magnitude at lower temperatures, under the influence of a *dc* bias voltage in the range of ~33 to 200 Vcm^{-1}, with conductivity values in the range ~$(1–2)\times10^{-2}$ Scm^{-1} at room temperature and almost zero activation energy. The onset voltage for conductivity enhancement decreases with increasing temperature and the conductivity increase is reversible, with hysteresis, on removal of the *dc* bias.

The mechanism associated with the conductivity increase is independent of electrode material and is associated with both the bulk and grain boundary regions of the ceramics. Thus, the impedance of BCF30 corresponds to that of the bulk, with no significant contribution from either grain boundaries or sample-electrode contacts in the *OFF* state, although the bulk impedance arc in the high conductivity, *ON* state is outside the frequency range of the available instrumentation. Since BCF30 is electrically homogeneous in the *OFF* state, there is no need to consider the possibility of alternative conduction pathways, avoiding the bulk, in the *ON* state and, indeed, as the conduction is isotopic, there is no evidence of any filamentary conduction. For BCF05, the grain boundary impedance is greater than that of the bulk and both show a bias dependence before the *ON* state is reached. It is not clear why a separate grain boundary impedance is seen with BCF05, but not with BCF30. This may be related to the lower symmetry of BCF05, as well as the possibilities of dimensional changes associated with a phase transition during post-sinter cooling or variations in oxygen content of grains and grain boundaries; further work would be required to clarify why a grain boundary impedance is sometimes observed.

Recently, Rubi *et al.* [**11,12**] observed resistive-switching in $Bi_{0.9}Ca_{0.1}FeO_3$ ceramics and attributed it to a variation of the Schottky potential barrier height at the sample–electrode interface, i.e. the material behaved as a metal–oxide varistor. The effect was attributed to oxygen vacancy migration to/from the metal–oxide interface. The field-enhanced conductivity data reported here are not associated with an interfacial varistor effect. Thus, the impedance data, **Figure 1**, show no evidence of an impedance associated with a Schottky barrier at the metal–oxide interface; instead, the magnitudes of the associated permittivities indicate that the conductivity variations are associated with bulk and grain boundary regions of the sample.

The field-enhanced conductivity observed here is different from that seen with TiO_2 -based thin layer memristor devices [**2,3**]. In memristors, coupled electromigration of oxygen vacancies (i.e. ionic transport) and electrochemical redox electron transfer between Ti^{4+} and Ti^{3+}, are proposed to occur under an electric field leading the device into its *ON* state. On removing the bias, the *ON* state

is maintained since the mobility of the oxygen vacancies at room temperature is very low. Consequently, a reverse bias is required to drive the memristor into its *OFF* state.

In our experiments, the material returns to its ground state within a few minutes on removal of the *dc* bias, **Figures 5–7**. This could indicate that the mobility of the oxygen vacancies is unusually large. However, the time taken to achieve the steady state with *dc* bias just above the onset voltage is significantly greater than the subsequent recovery time after removing the *dc* bias, **Figure 5**, in contradiction to the expectation that drift of oxygen vacancies would be enhanced in an electric field. There is also no evidence from the impedance data, **Figure 1**, for any low frequency effects, such as charge transfer impedances or Warburg impedances, which are a characteristic of oxide ion conduction. We conclude, therefore, that oxide ion conduction (or oxide vacancy conduction), if it occurs at all, is not the main driver for the observed conductivity changes.

From the results presented above, the conductivity is non-ohmic in the sense that the carrier concentration must be bias-dependent. In general, conduction in bulk materials is ohmic at low fields but may become non-ohmic at high fields if carrier injection from the electrode occurs [**16**]. The electrical properties reported here show ohmic contacts at the sample-electrode interfaces, **Figure 1**, a *p*-type bulk conduction mechanism and enhanced electrical conductivity, **Figures 4** and **7**, at fields as low as 3.3 V/mm. Additional unusual features are the time delay before switching between *ON* and *OFF* states, leading to hysteresis and a more rapid switch, under certain conditions, in the *ON*-*OFF* direction than in the reverse direction. A new mechanism is required, and proposed, to explain this effect since none of the existing models can account for the observations reported here. This is shown schematically in **Figure 11**; it is based on earlier studies of voltage-dependent conductivity in perovskite-structured, acceptor-doped titanates of Ba, Sr and Ca [**17–22**].

First, a key requirement is that the material is acceptor-doped since undoped $BiFeO_3$ does not show any significant voltage-dependence of its resistance (not shown). The defect structure of Ca-doped $BiFeO_3$ consists of a disordered distribution of dopant Ca^{2+} ions on Bi^{3+} sites and oxygen vacancies which tend to associate with the Ca^{2+} dopants to preserve local electroneutrality, **Figure 11(a)**. In the cases of acceptor-doped titanates [**17–22**], the dopant substitutes partially for Ti^{4+} on the B sites whereas here, Ca substitutes for Bi on the A sites.

Second, the *p*-type conductivity is enhanced under a dc bias and therefore, requires a source of holes; from our previous studies in doped alkaline earth titanates this is attributed to underbonded

O^{2-} ions in the crystal lattice which are able to ionise readily to give O^- ions. The only realistic alternative source of holes in BCF materials is Fe^{3+} since the non-transition metal cations that are present cannot be oxidised any further. In all the various doped alkaline earth titanates [**17–22**], however, none of the metal cations present could be oxidised as a source of holes and it is unlikely that a transition metal impurity was present in the doped materials but not in the undoped parent materials. In Ca-doped $BiFeO_3$, hole creation in the form of Fe^{4+} ions is, in principle, an alternative charge compensation mechanism to creation of oxygen vacancies, but there is strong evidence for oxide ion conduction and therefore, for oxygen vacancy creation as the main charge compensation mechanism [**13**]. Nevertheless, the conduction mechanism in slowly-cooled BCF samples is *p*-type [**13**] and the possibility exists that this is attributable either to Fe^{4+}ions or to O^- ions.

Third, the underbonded oxygens are associated with the acceptor dopants. In the titanates, the dopants substitute for Ti^{4+} on the B sites of the perovskite lattice and therefore, the surrounding oxygens experience less positive charge than those in a fully stabilised crystal lattice. In Ca-doped $BiFeO_3$, the oxide ions that have Ca^{2+} ions on Bi sites in their first coordination sphere are also underbonded. We recall that the O^{2-} ion is thermodynamically unstable in the gas phase and should spontaneously ionise whereas in a crystal lattice, it is stabilised by the extra lattice energy associated with doubly-charged O^{2-} ions in comparison with singly-charged O^- ions. In any crystalline environment in which O^{2-} ions are not surrounded by a full complement of effective positive charge 2+, their ready ionisation is a possibility.

Fourth, the driving force for ionisation of underbonded oxide ions, especially those near the sample surface, on application of a dc bias, comes from changes to the equilibria between various oxygen species at the sample surface. Specifically, at the anode (positively-charged electrode) some, or all, of the equilibria in the following scheme are displaced to the right hand side:

$$O_2(g) \leftrightarrow O_2(ads) \leftrightarrow O^-_2 \leftrightarrow O_2^{2-}/O^- \leftrightarrow O^{2-}\,(surface) \leftrightarrow O^{2-}\,(bulk) \qquad (1)$$

Consequently, electrons are withdrawn from the near-surface, sample interior and are trapped at the sample surface as increasingly-reduced oxygen species. With time and commencing at the sample surface, further underbonded oxide ions, deeper within the sample interior, progressively ionise leading to the thickening of a positively-charged region containing a non-equilibrium excess of holes, **Figure 11(b)**.

Fifth, a process of capacitive charging takes place, facilitated by charge transfer between the increasingly-conductive 'dielectric' and the anode. Charge is stored initially at the anode surface and within the positively-charged dielectric. The rate of charging decreases initially with thickening of the positively-charged dielectric, but subsequently, accelerates rapidly as the positively-charged, highly-conducting 'dielectric' approaches the cathode surface, **Figure 11(c)**. Finally, the total sample conductivity becomes that of the material with an increased hole concentration and is several orders of magnitude higher than that of the material in its original, uncharged state.

The net effect of application of a *dc* bias to Ca-doped $BiFeO_3$ ceramics is that the sample-electrode combination becomes, effectively, a charged and increasingly leaky capacitor; ionisation of a previously-neutral material gives rise to a negatively-charged anode and a positively-charged medium between the electrodes. The high conductivity state is retained until the bias is reduced to below the twilight voltage at which point, the changes to the surface equilibria shown in scheme (1) are reversed, the released electrons diffuse back into the sample and recombine rapidly with the O^- ions. The response time in the *ON-OFF* direction is more rapid than in the charging, *OFF-ON* direction since the activation energy for ionisation of underbonded oxide ions does not need to be overcome: by contrast, recombination is a spontaneous process for which there is no activation barrier.

The enhanced conductivity of the bias-dependant steady state is isotropic because the Ca acceptors and the associated under-bonded O^{2-} ions are randomly distributed through the crystal structure; consequently, the conduction pathways are not filamentary in nature. The process is driven by a charging mechanism initiated at the anode-sample interface but is not associated with Schottky barriers that may form spontaneously at sample-metal interfaces, across which there is a significant difference in Fermi level. The voltage dependence is therefore a material phenomenon exhibited by both bulk and grain boundary regions rather than a potential barrier associated with contacts between dissimilar materials.

It is possible that the above mechanism may represent the first step in other, more complex memristive processes. Thus, it does not require oxide ion (or vacancy) transport, although this is suggested to be a key requirement in other memristive studies [**23–31**]. It does not require electron injection at the cathode, although evidence for this has been obtained from electrocolouration effects in other materials [**23–31**]. It does not require a cation-based mechanism for hole creation at the anode-sample interface; this is important since there may be no obvious cationic species that could act as a source of holes (Fe in $BiFeO_3$ is, arguably, an exception). The capacitive nature of the

ON/*OFF* switching indicates that, while ionisation of underbonded oxygens occurs during charging, this does not have the characteristics of a complete redox reaction typical of an electro-chemical process in which an oxidation reaction occurs at one electrode and a reductive process at the opposite electrode.

The results reported here on Ca-doped $BiFeO_3$ are different in nature but not in mechanism from that seen with various acceptor-doped titanate perovskites [**17–22**]. In the present case, the *ON*/*OFF* switching occurs at much lower temperatures and more rapidly than in the titanates. Certainly, the level of electronic conduction is much higher for Ca-doped $BiFeO_3$ and ionisation of the underbonded oxide ions appears to be much easier. The concentration of underbonded oxide ions is also much larger since the materials contain 5-30% Ca whereas the titanates had ≤ 1% of acceptor dopant. This raises the fascinating possibility that the ionisation of underbonded oxide ions may vary greatly between different materials. At one extreme, oxide ions are fully stabilised within the crystal lattice and do not exhibit preferred or easy ionisation. At the other extreme, the activation barrier to ionisation of underbonded oxide ions may be low or even zero, leading to novel switching effects and high conductivities.

On application of a *dc* bias to $Bi_{1-x}Ca_xFeO_{3-x/2}$ samples, two possible processes may be visualised to occur simultaneously: both holes and oxygen vacancies, $V_O^{\bullet\bullet}$, drift towards the –ve electrode; alternatively, and equivalently, electrons and oxide ions, $O_O^{\times}$, drift towards the +ve electrode. There is no evidence from low frequency impedance data that transfer of oxygen occurs at either sample-electrode interface; instead, capacitive charge build-up occurs. We cannot exclude the possibility that oxide ion transport contributes to the bias-dependent enhanced conductivity, but it is not an essential requirement. On application of the dc bias, however, electron ionisation must occur in the vicinity of the positive electrode, with subsequent trapping of the ionised electrons. The species responsible for the ionised electrons could be Fe^{3+} which ionise to Fe^{4+} or alternatively, O^{2-} which ionise to O^-. There is strong evidence from bias-dependence effects in acceptor-doped $ATiO_3$:A = Ca, Sr, Ba, that O^- ions are the hole carriers since there are no transition metal ions present in the materials. In the present materials, we propose that O^{2-} ions are also the main source of holes but cannot exclude the possibility that Fe^{3+} ions are also involved in some way.

Although the $Bi_{1-x}Ca_xFeO_{3-x/2}$ materials are predominantly *p*-type semiconductors, they do exhibit significant levels of oxide ion conduction at high temperatures, as a minority process during measurements in air. Further, at lower pO_2, such as during measurements in N_2, the *p*-type conduction is greatly reduced since desorption of O_2 molecules from the sample surface (present as

partially-ionised oxygen species) leads to electron injection which cancels the *p*-type conduction. As a consequence, oxide ion conduction becomes the predominant mechanism and high levels of conductivity are observed, comparable to that in yttria-stabilised zirconia [**13**].

Conclusions

1.The *p*-type semiconductivity of Ca (acceptor) – doped $BiFeO_3$ ceramic can be increased, reversibly, at room temperature by 3 orders of magnitude on application of a small *dc* bias in the range 3 to 30 V/mm. The effect is shown by both grains and grain boundaries of the ceramics, is independent of electrode material and is not associated with interfacial Schottky barriers. In the state of enhanced conductivity, the conductivity is essentially unchanged, with zero activation energy, down to –253 ^{o}C.

2. A novel mechanism is proposed for this effect which involves a combination of capacitive charging and internal ionisation; charge is stored by trapping ionised electrons at the sample (anode) surface and the creation of positively-charged grain interiors which are believed to be associated with holes located on oxygen as O^- ions.

3. The enhanced conductivity under a *dc* bias is isotropic and therefore different in nature from the filamentary conduction that has been proposed for memristive switching effects in other materials. It also does not require electrochemical redox reactions to occur at sample-electrode interfaces which are reversible only under the application of a reverse bias.

4. The key materials requirement appears to be the presence of underbonded oxygens associated with acceptor dopants, in this case with Bi substituted partially by Ca. Similar phenomena, but occurring over much longer timescales and only at high temperatures, have been observed previously in acceptor-doped perovskites, $ATiO_3$: A = Ba, Sr, Ca, in which Ti is replaced partially by divalent elements such as Mg, Zn.

Acknowledgements

We thank the EPSRC for financial support.

References

[1] L. O. Chua, “Memristor – The missing circuit element”, *IEEE Trans. Circ.Theory*, 1971, **18**[5] 507–519.

[2] D. B. Strukov, G. S. Snider, D. R. Stewart and R. S. Williams, "The missing memristor found" *Nature*, 2008, **453**, 80–83.

[3] J. M. Tour and T. He, "The Fourth Element", *Nature*, 2008, **453**, 42–43.

[4] G. Dearnaley, A. M. Stoneham and D. V. Morgan, "Electrical phenomena in amorphous oxide films", *Rep. Prog. Phys.*, 1970, **33**, 1129–1191.

[5] D. P. Oxley, "Electroforming, switching and memory effects in oxide thin films", *Electrocomponent Sci. Technol. UK*, 1977, **3**, 217–224.

[6] H. Pagnia and N. Sotnik, "Bistable switching in electroformed metal-insulator-metal devices", *Phys. Status Solidi*, 1988, **108**[1], 11–65.

[7] A. Asamitsu, Y. Tomioka, H. Kuwahara and Y. Tokura, "Current switching of resistive states in magnetoresistive manganates", *Nature*, 1997, **388**, 50–52.

[8] A. Beck, J. G. Bednorz, Ch. Gerber, C. Rossel and D. Widmer, "Reproducible switching effect in thin oxide films for memory applications", *Appl. Phys. Lett.*, 2000, **77**[1], 139–141.

[9] R. Waser and M. Aono, "Nanoionics-based resistive switching memories", *Nature Mater.*, 2007, **6**, 833–840.

[10] J. J. Yang, M. D. Pickett, X. Li, D. A. A. Ohlberg, D. R. Stewart and R. S. Williams, "Memristive switching mechanism for metal/oxide/metal nanodevices", *Nature Nanotechnology*, 2008, **3**, 429–433.

[11] D. Rubi, F. Gomez-Marlasca, P. Bonville, D. Colson and P. Levy, "Resistive switching in ceramic multiferroic $Bi_{0.9}Ca_{0.1}FeO_3$", *Physica B*, 2012, **407**[16], 3144–3146.

[12] D. Rubi, F.G. Marlasca, M. Reinoso, P. Bonville, P. Levy, "Magnetism and electrode dependant resistive switching in Ca-doped ceramic bismuth ferrite", *Mat. Sci. Eng. B*, 2012, **177**[6], 471– 475.

[13] N. Masó and A. R. West, "Electrical properties of Ca-doped $BiFeO_3$ ceramics: from *p*-type semiconduction to oxide-ion conduction", *Chem. Mater.*, 2012, **24**[11], 2127−2132.

[14] W.-T. Chen, A. J. Williams, L. Ortega-San-Martin, M. Li, D. C. Sinclair, W. Zhou and J. P. Attfield, "Robust antiferromagnetism and structural disorder in $Bi_xCa_{1-x}FeO_3$ perovskites", *Chem. Mater.*, 2009, **21**[10], 2085–2093.

[15] J. Schiemer, R. Withers, L. Norén, Y. Liu, L. Bourgeois and G. Stewart, "Detailed phase analysis and crystal structure investigation of a $Bi_{1-x}Ca_xFeO_{3-x/2}$ perovskite-related solid solution phase and selected property measurements thereof", *Chem. Mater.*, 2009, **21**[18], 4223–4232.

[16] K. C. Kao in *Dielectric phenomena in solids: with emphasis on physical concepts of electronic processes*, Elsevier Academic Press (2004).

[17] M. Prades, N. Masó, H. Beltrán, E. Cordoncillo and A.R. West, "Field enhanced bulk conductivity of $BaTiO_3$:Mg ceramics", *J. Mater. Chem.*, 2010, **20**[25], 5335–5344.

[18] H. Beltrán, M. Prades, N. Masó, E. Cordoncillo and A.R. West, "Voltage-dependent low-field bulk resistivity of $BaTiO_3$:Zn ceramics", *J. Am. Ceram. Soc.*, 2010, **93**[2], 500–505.

[19] N. Masó, M. Prades, H. Beltrán, E. Cordoncillo, D.C. Sinclair and A.R. West, "Field enhanced bulk conductivity of acceptor doped $BaTi_{1-x}Ca_xO_{3-x}$ ceramics", *App. Phys. Lett.*, 2010, **97**[6], 062907.

[20] H. Beltrán, M. Prades, N. Masó, E. Cordoncillo and A.R. West, "Enhanced conductivity and non-linear voltage-current characteristics of non-stoichiometric $BaTiO_3$ ceramics", *J. Am. Ceram. Soc.*, 2011, **94**[9], 2951–2962.

[21] Q-L Zhang, N. Masó, Y. Liu, H. Yang and A.R. West, "Voltage-dependent low-field resistivity of $CaTiO_3$:Zn ceramics", *J. Mater. Chem.*, **21**[34], 12894–12900.

[22] L. Gil-Escrig, M. Prades, H. Beltrán, E. Cordoncillo, N. Masó and A. R. West, "Voltage-Dependent Bulk Resistivity of $SrTiO_3$:Mg Ceramics", J. Am. Ceram. Soc., in press, DOI: 10.1111/jace.34147 (2014).

[23] R. Waser, T. Baiatu and K.H. Härdtl, "Degradation of dielectric ceramics", *Mat. Sci. Eng A*, 1989, **109**, 171–182.

[24] J. Blanc and D.L. Staebler, "Electrocoloration in $SrTiO_3$: Vacancy drift and oxidation-reduction of transition metals", *Phys. Rev. B*, 1971, **4**, 3548–3557.

[25] S. K. Mohapatra and S. Wagner, "Electrochromism in nickel-doped strontium titanate", *J. Appl. Phys.*, 1979, **50**[7], 5001–5006.

[26] W.A. Schulze, L.E. Cross and W.R. Buessem, "Degradation of $BaTiO_3$ ceramic under high ac electric field", *J. Am. Ceram. Soc.*, 1980, **63**[1–2], 83–87.

[27] R. Waser, "Electrochemical boundary conditions for resistance degradation of doped alkaline-earth titanates," J. Am. Ceram. Soc., 1989, **72**[12], 2234–2240.

[28] R. Waser, T. Baiatu and K.H. Härdtl, "dc electrical degradation of perovskite-type titanates: I, Ceramics", *J. Am. Ceram. Soc.*, 1990, **73**[6], 1645–1653; "II, Single crystals", *J. Am. Ceram. Soc.*, 1990, **73**[6], 1654–1662; "III, A model of the mechanism", *J. Am. Ceram. Soc.*, 1990, **73**[6], 1666–1673.

[29] S. Rodewald, J. Fleig and J. Maier, "Resistance degradation of iron-doped strontium titanate investigated by spatially resolved conductivity measurements", *J. Am. Ceram. Soc.*, 2000 **83**[8], 1969–1976.

[30] S.H. Yoon, C.A. Randall and K.H. Hur, "Effect of acceptor (Mg) concentration on the resistance degradation behavior in acceptor (Mg)-doped $BaTiO_3$ bulk ceramics: I. Impedance Analysis", *J. Am. Ceram. Soc.*, 2009, **92**[8], 1758–1765 (2009); "II. Thermally Stimulated Depolarization Current Analysis", *J. Am. Ceram. Soc.*, 2009, **92**[8], 1766–1772.

[31] S.H. Yoon, C.A. Randall and K.H. Hur, “Influence of grain size on impedance spectra and resistance degradation behavior in acceptor (Mg)-doped $BaTiO_3$ Ceramics”, *J. Am. Ceram. Soc.*, 2009, **92**[12], 2944–2952.

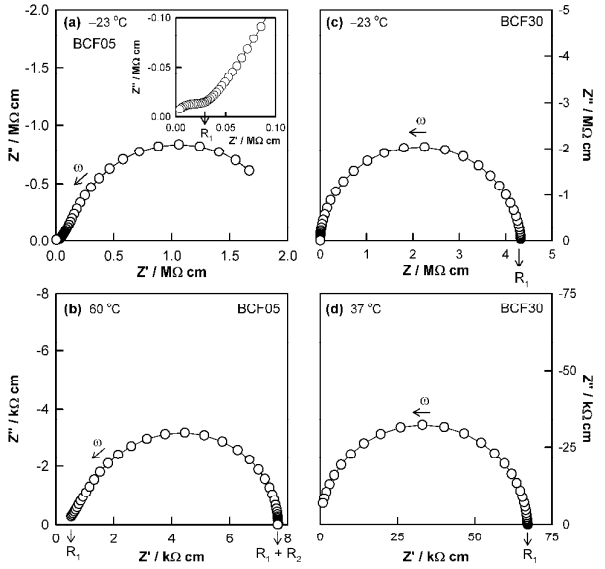

Figure 1. Impedance complex plane plots at several temperatures for BCF05 (a,b) and BCF30 (c,d). Angular frequency, $\omega = 2\pi f$.

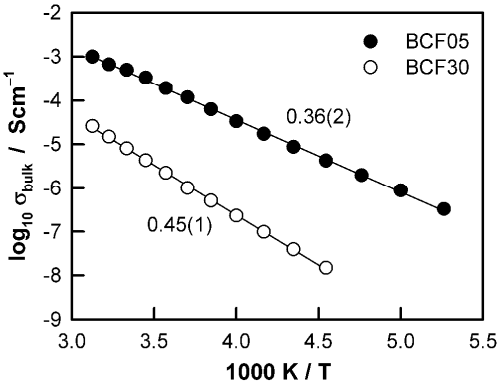

Figure 2. Bulk Arrhenius plots for $Bi_{1-x}Ca_xFeO_{3-x/2}$ ceramics. Activation energies, in eV, are noted beside each data set.

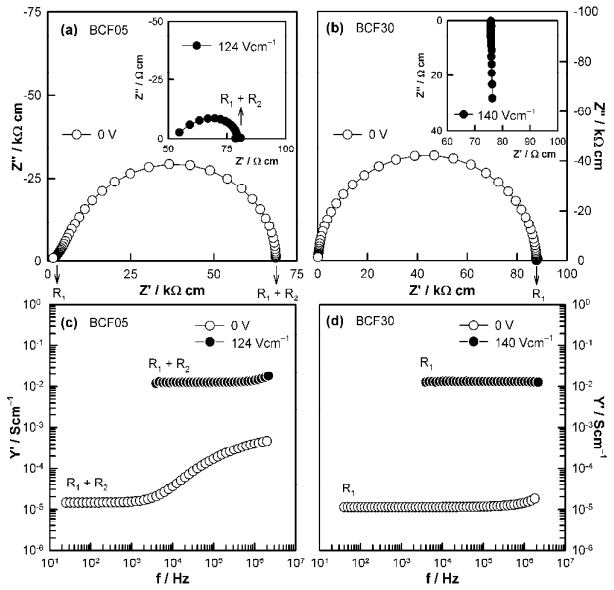

Figure 3. Impedance complex plane plots (a,b) and Y' spectroscopic plots (c,d) at ~30 ^{o}C before and after a voltage was applied.

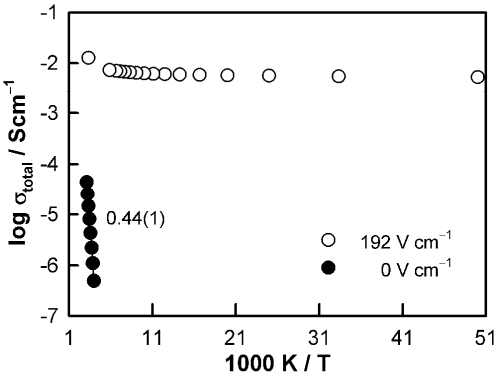

Figure 4. BCF05: Arrhenius plots of total conductivity measured without a *dc* bias and with an applied voltage of 192 Vcm^{-1} after a steady state had been reached.

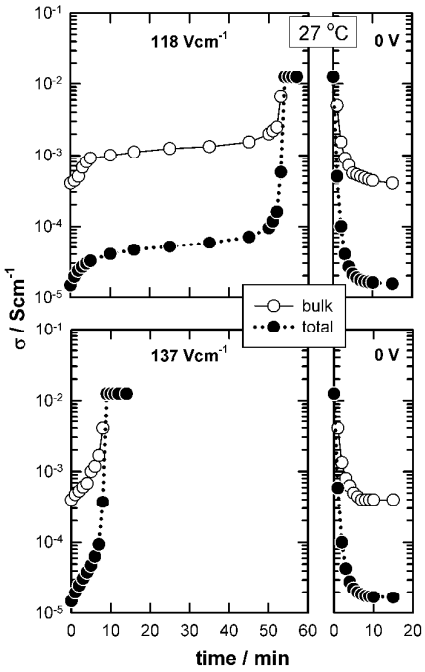

Figure 5. BCF05: bulk and total conductivity at 27 °C *vs* time after different voltages were applied.

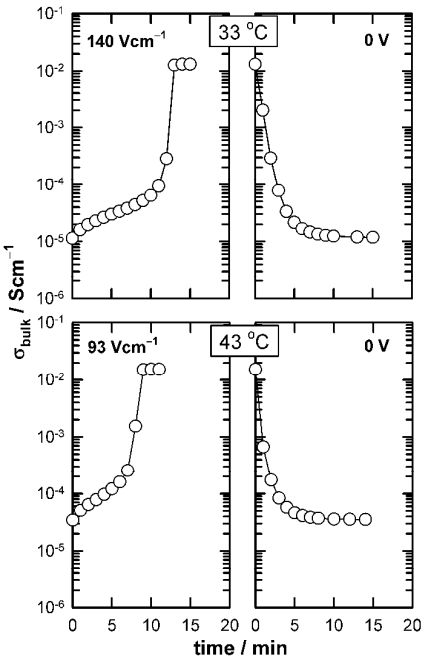

Figure 6. BCF30: bulk conductivity at two temperatures *vs* time after different voltages were applied.

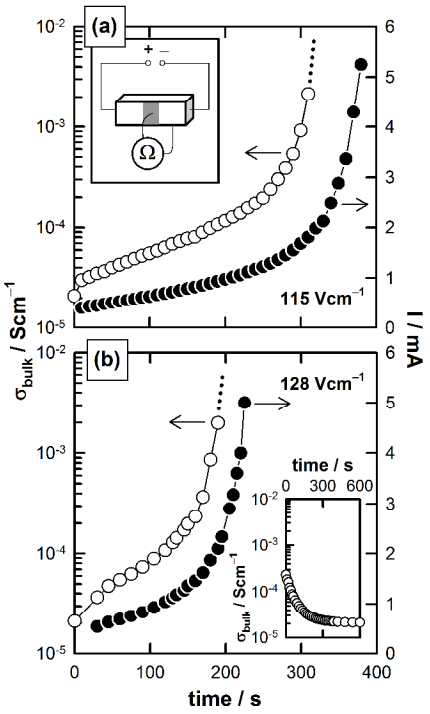

Figure 7. BCF30: *dc* conductivity and current perpendicular and parallel to the direction of the applied voltage, respectively, against time for several *dc* bias voltages at ~50 °C. Inset in (a): schematic setup for *dc* conductivity measurements perpendicular to the direction of the *dc* bias. Inset in (b): *dc* conductivity *vs* time on removal of the *dc* bias.

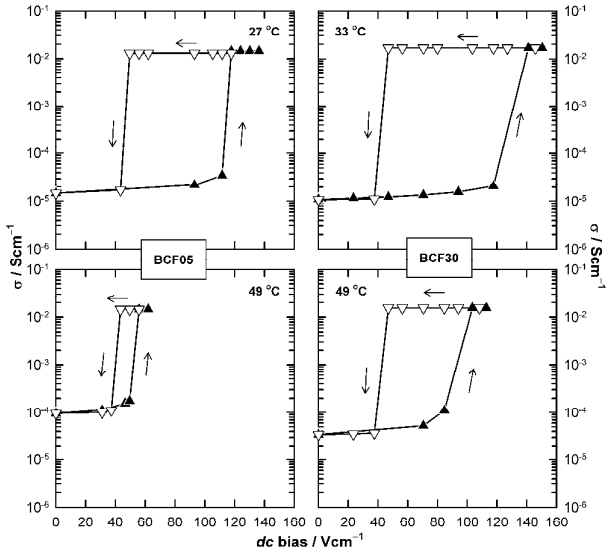

Figure 8. Total conductivity after a steady state had been reached *vs* applied voltage at two temperatures for compositions BCF05 and BCF30.

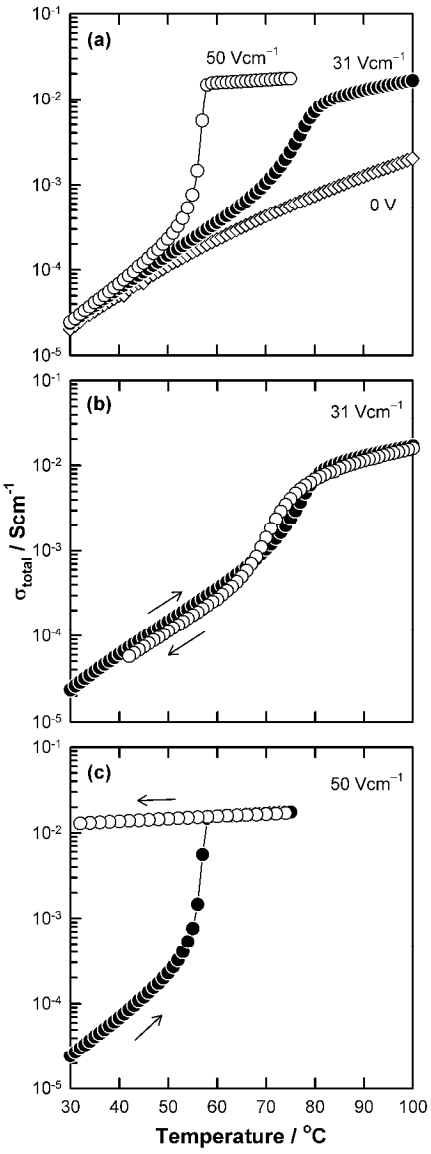

Figure 9. BCF05: total conductivity *vs* temperature after a range of voltages was applied.

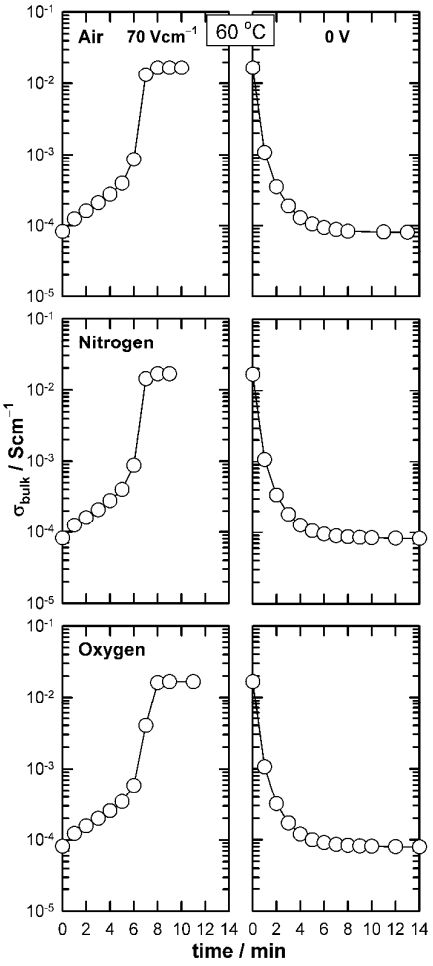

Figure 10. BCF30: bulk conductivity *vs* time in air, nitrogen and oxygen.

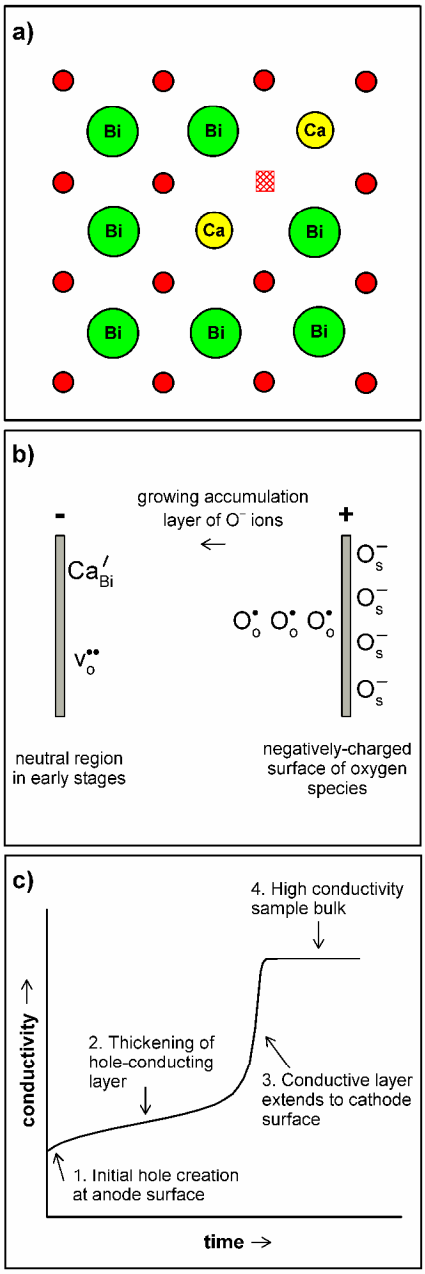

Figure 11. (a) Defect structure for $Bi_{1-x}Ca_xFeO_{3-x/2}$, (b) capacitive model for voltage-dependent resistance and (c) schematic stages in capacitive charging process on application of a *dc* bias.